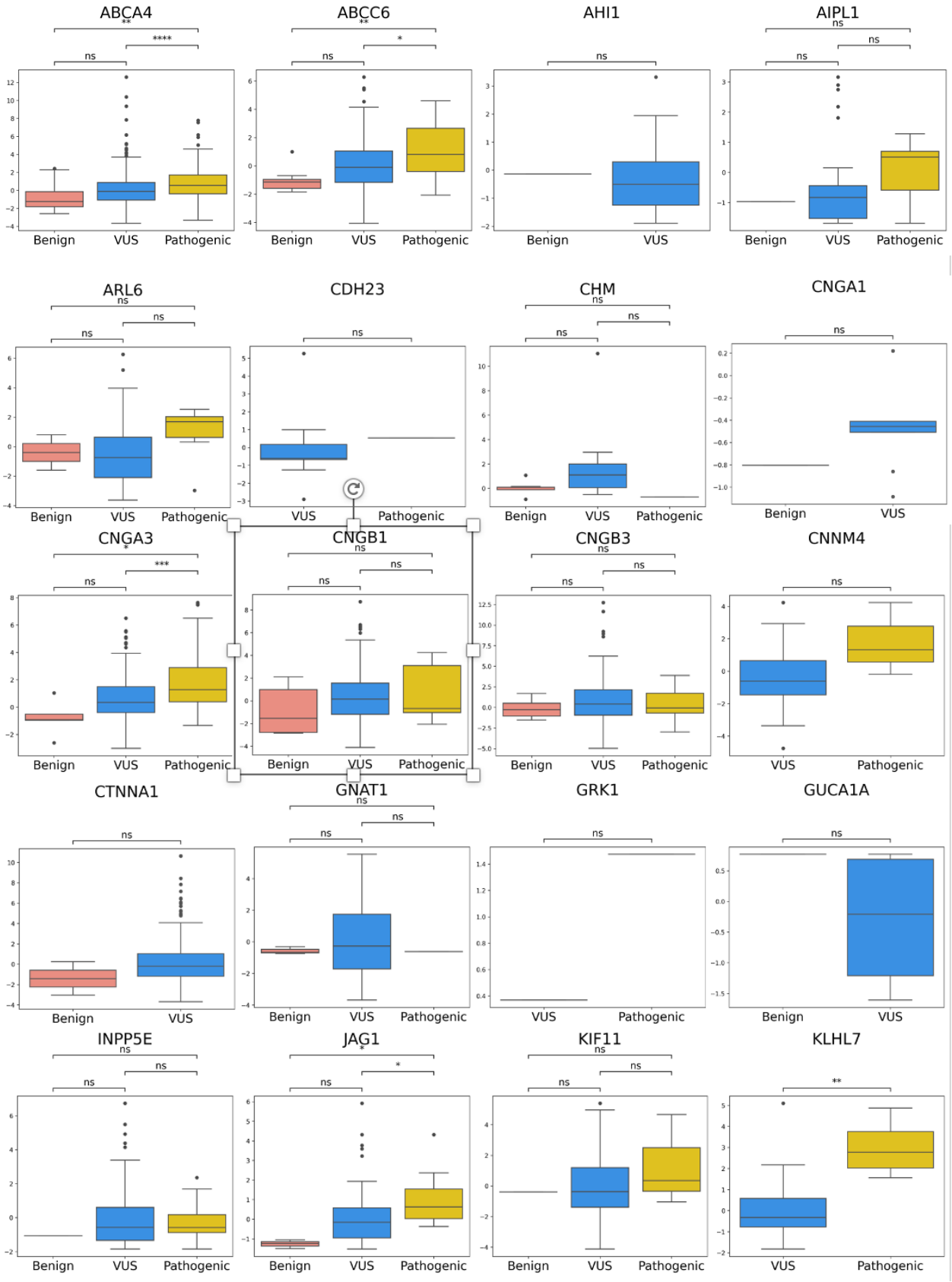
ABCA4
ABCC6
AHI1
AIPL1
ARL6
CDH23
CHM
CNGA1
CNGA3
CNGB1
CNGB3
CNNM4
CTNNA1
GNAT1
GRK1
GUCA1A
INPP5E
JAG1
KIF11
KLHL7
Benign
VUS
Pathogenic
ns

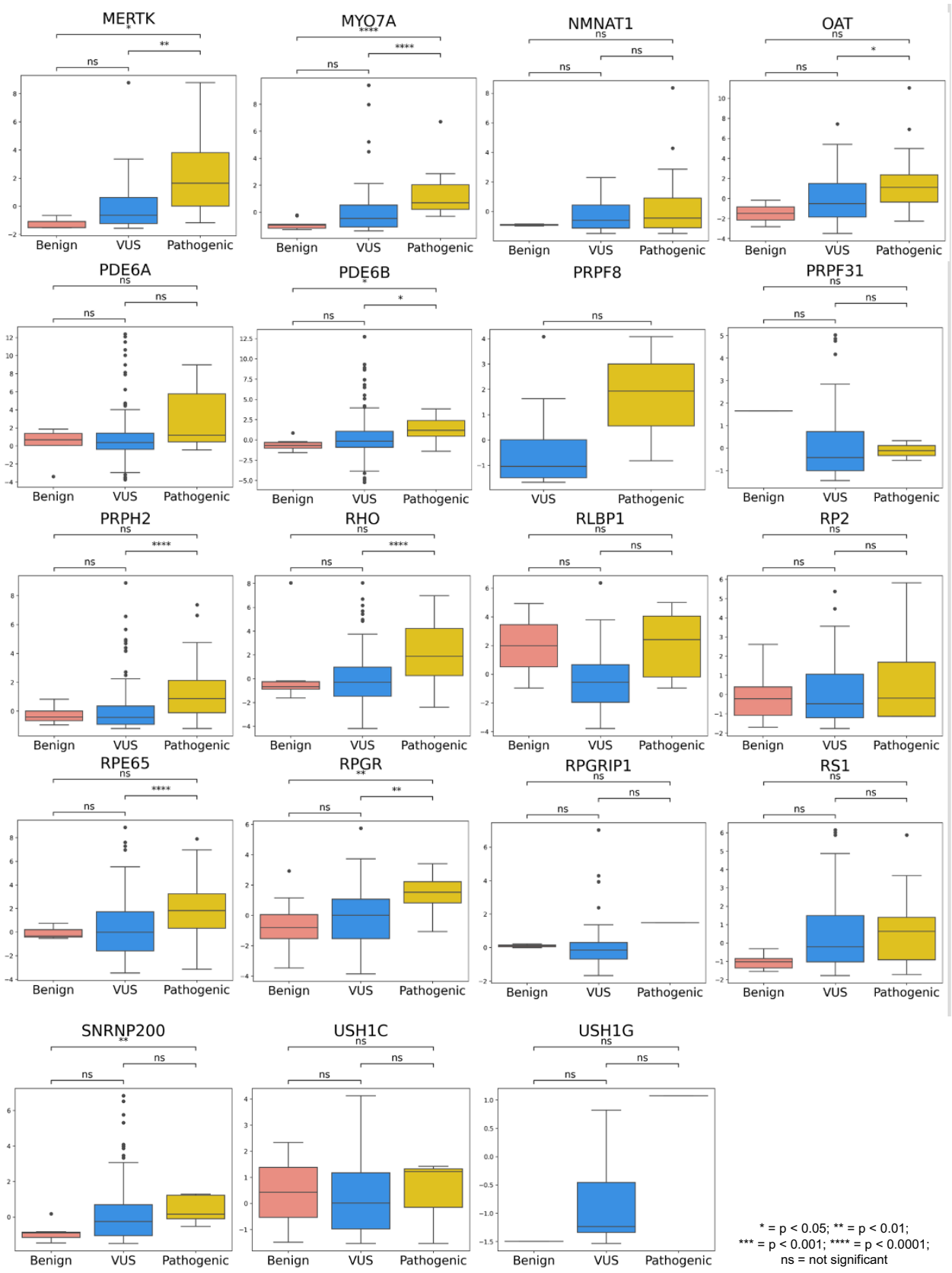
MERTK
MYO7A
NMNAT1
OAT
PDE6A
PDE6B
PRPF8
PRPF31
PRPH2
RHO
RLBP1
RP2
RPE65
RPGR
RPGRIP1
RS1
SNRNP200
USH1C
USH1G
Benign
VUS
Pathogenic
* = p < 0.05; ** = p < 0.01;
*** = p < 0.001; **** = p < 0.0001;
ns = not significant

Figure S1. Structure-based network analysis highlights pathogenic variants in individual inherited retinal disease proteins. Select individual comparisons between network scores for variants with available clinical phenotype data for inherited retinal disease proteins.

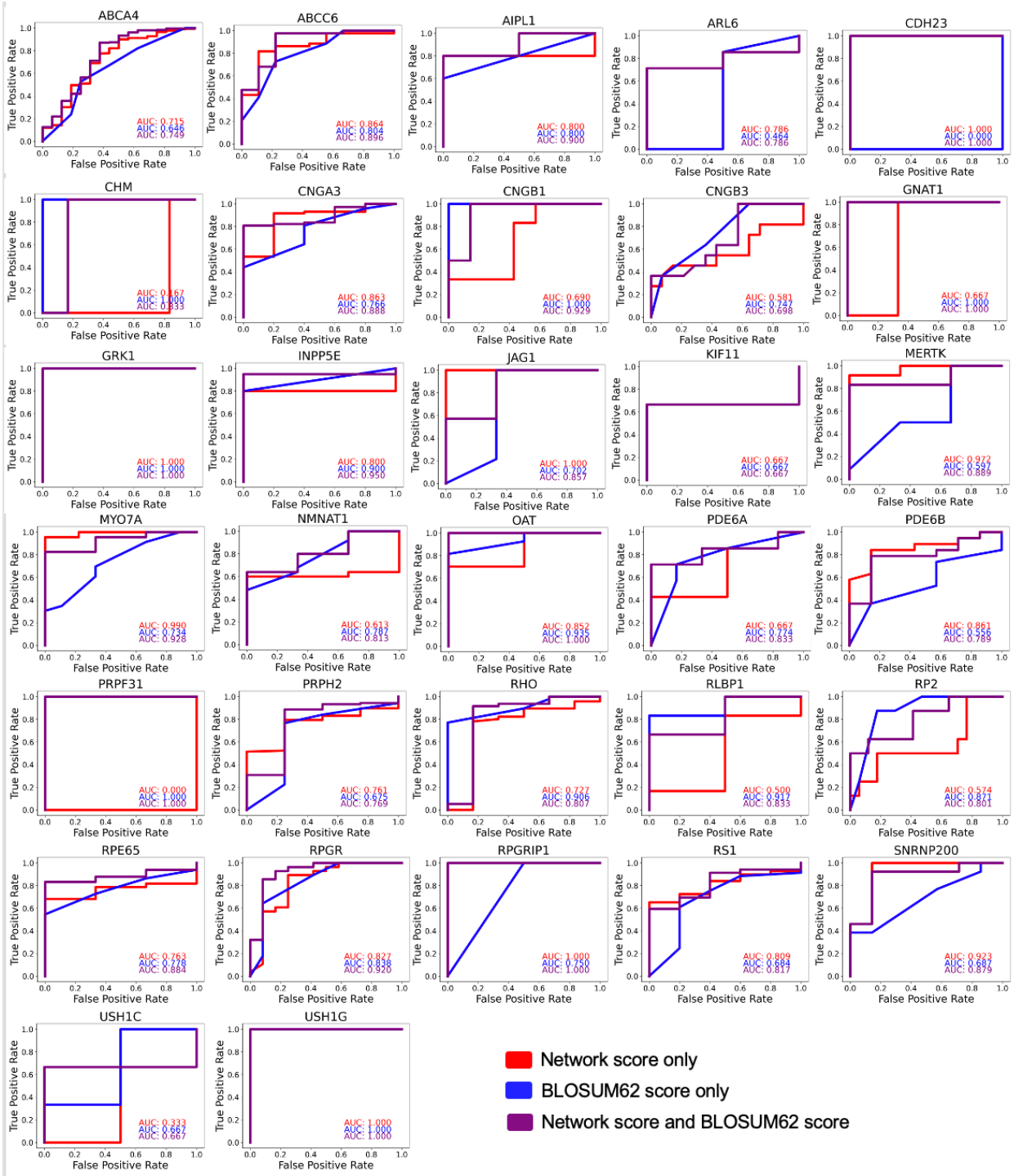

Figure S2. Logistic regression-based modelling using SBNA and BLOSUM62 is superior to univariate models for some individual proteins. Application of univariate and multivariable logistic regression models to the 32 inherited retinal disease proteins for which there was

sufficient data to facilitate individual analysis. All regressions were trained on all proteins except the protein of interest and then tested on that protein. AUC values are shown.

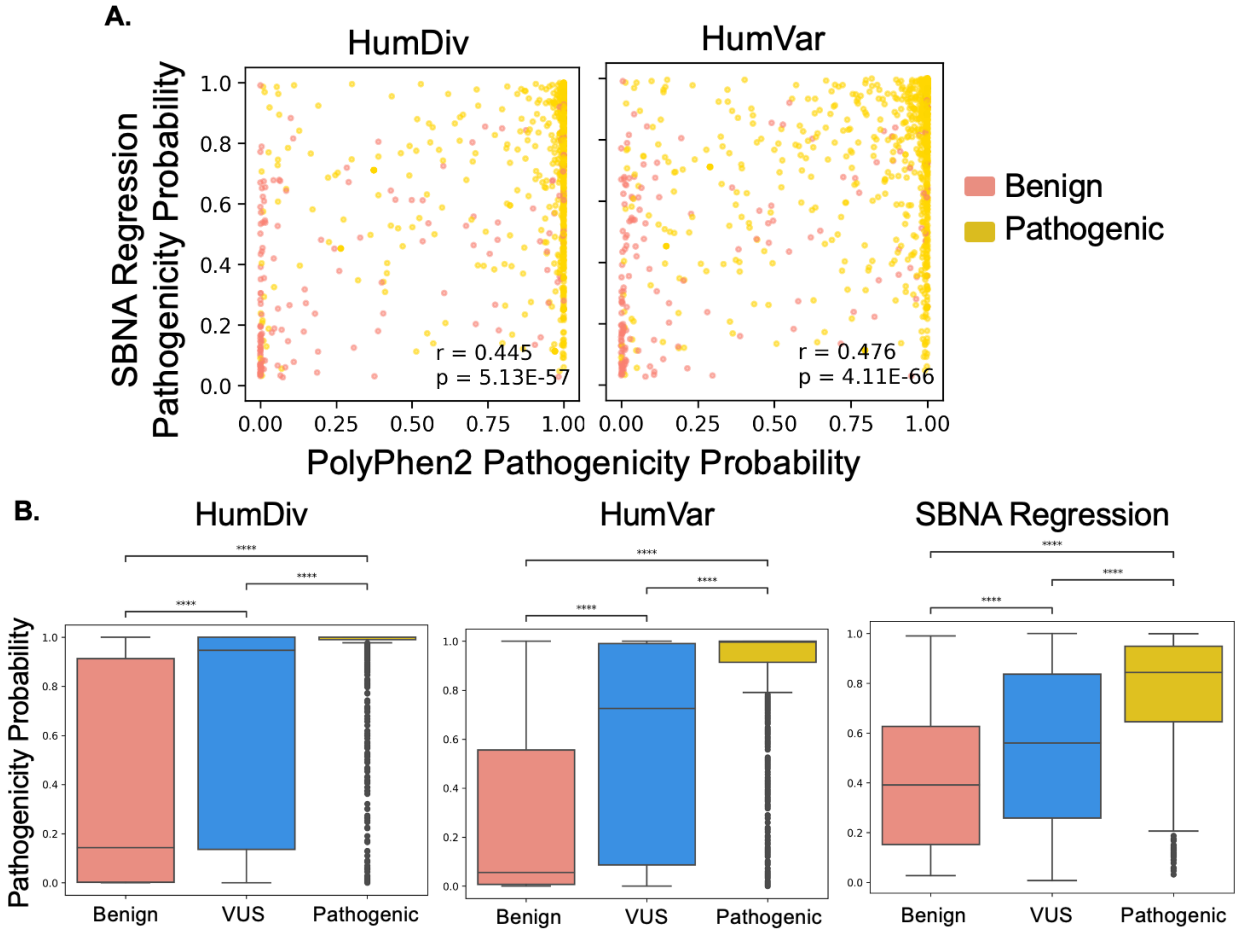

Figure S3. SBNA regression estimates show similar trends to estimates from PolyPhen2. **(A)** Comparison between pathogenicity probability estimates generated by the SBNA regression and PolyPhen2 trained on either the HumDiv or HumVar training data, with Spearman correlation coefficients displayed for each plot. **(B)** Comparison between pathogenicity probability estimates grouped by benign, VUS, and pathogenic variants as determined by ClinVar and gnomAD.

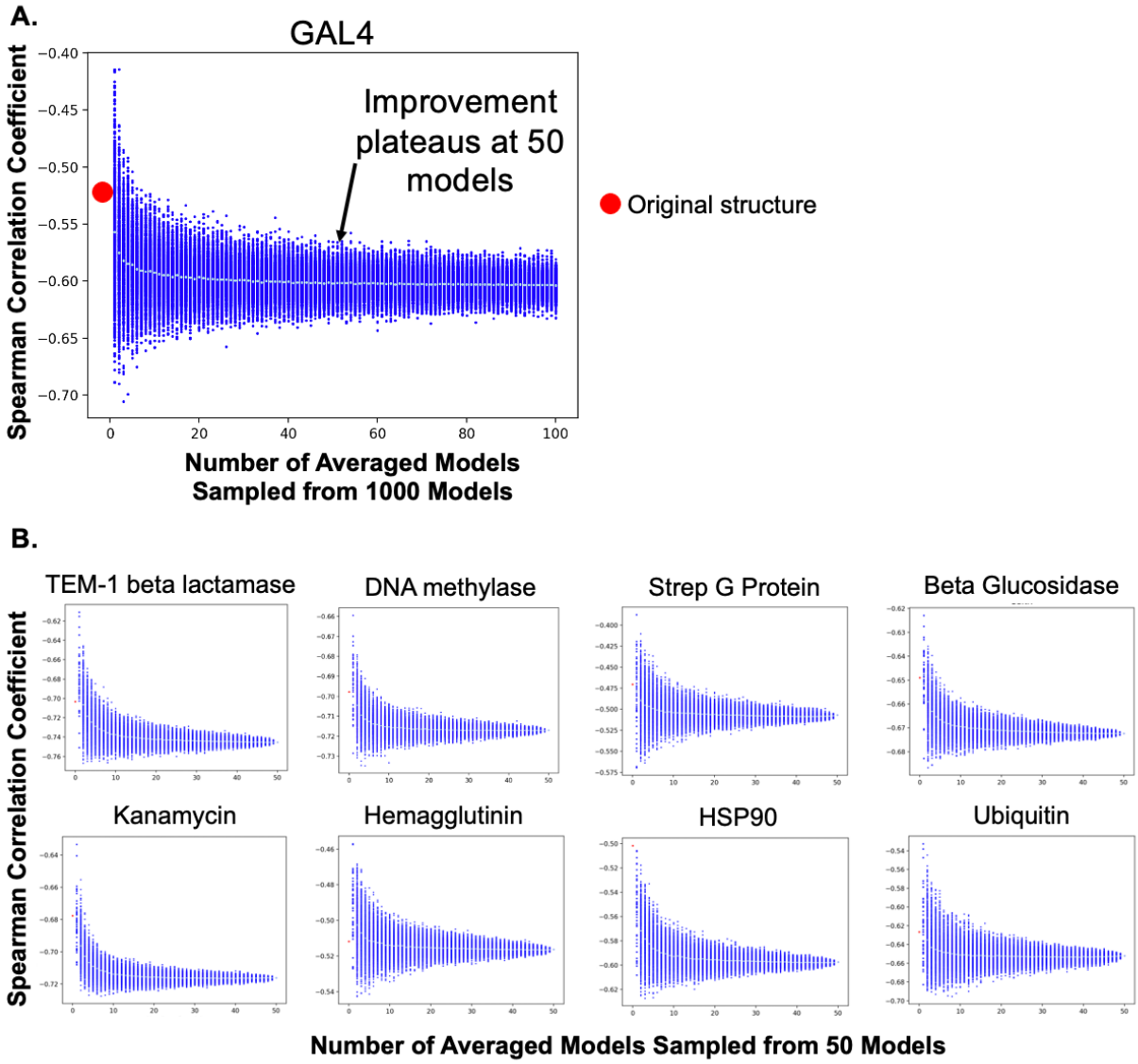

Figure S4. Homology modelling of benchmark proteins shows improvement in correlation between network scores and functional scores. (A) A threshold of 50 homology models was determined to be the point beyond which there was limited further improvement the Spearman correlation coefficient between network scores and functional scores from *in vitro* assays. **(B)** The effect of homology modelling on the Spearman correlation coefficient between network scores and functional scores from *in vitro* assays was measured across 8 additional benchmark proteins. Red dots depict the Spearman correlation coefficient for the original structure without homology modelling.

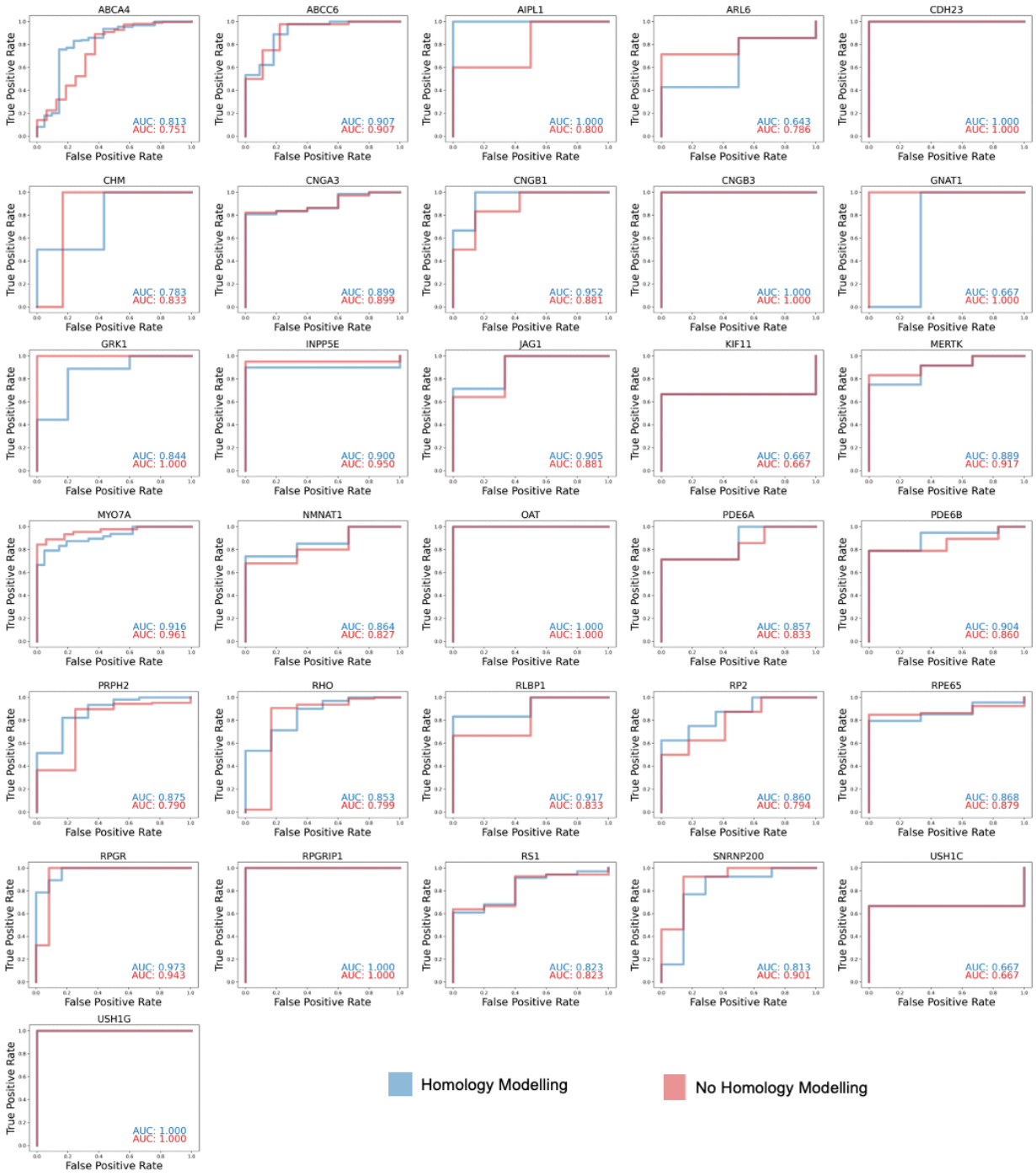

Figure S5. Multivariable logistic regressions with and without homology modelling show similar results. Application of the multivariable logistic regression model incorporating network scores and BLOSUM62 scores to 31 inherited retinal disease proteins. All regressions were

trained on all proteins except the protein of interest and then tested on that protein. AUC values are shown.

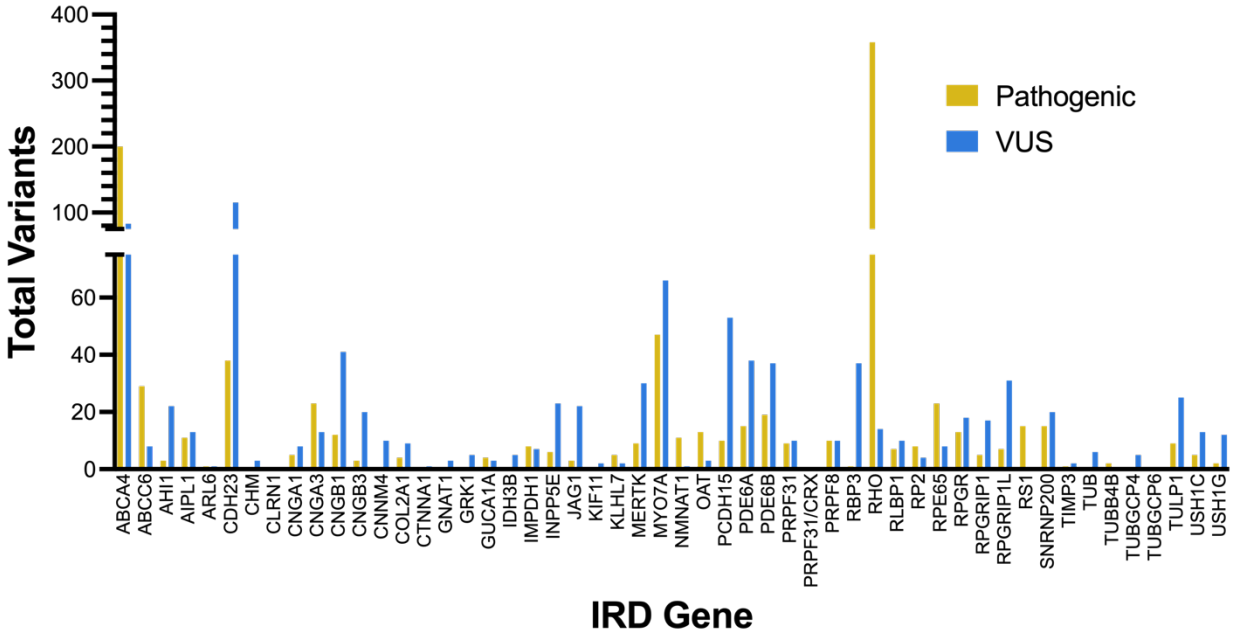

Figure S6. Pathogenic variants and VUS from MEE patients span 52 IRD genes.

Distribution of total pathogenic variants and VUS (as categorized by ClinVar) from MEE patients across the 52 IRD genes considered in this analysis.

A. Likely Solving Variants

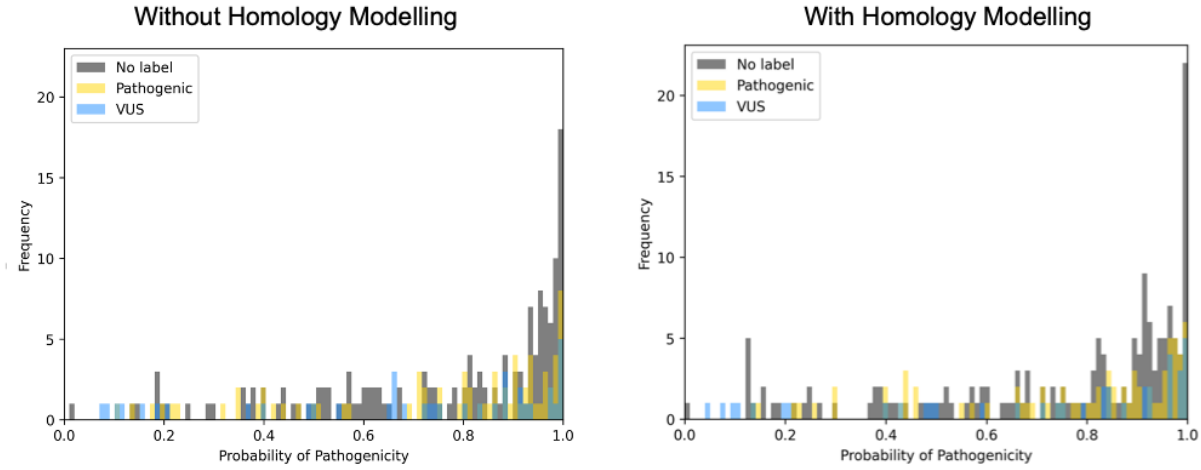

B. All Rare Variants

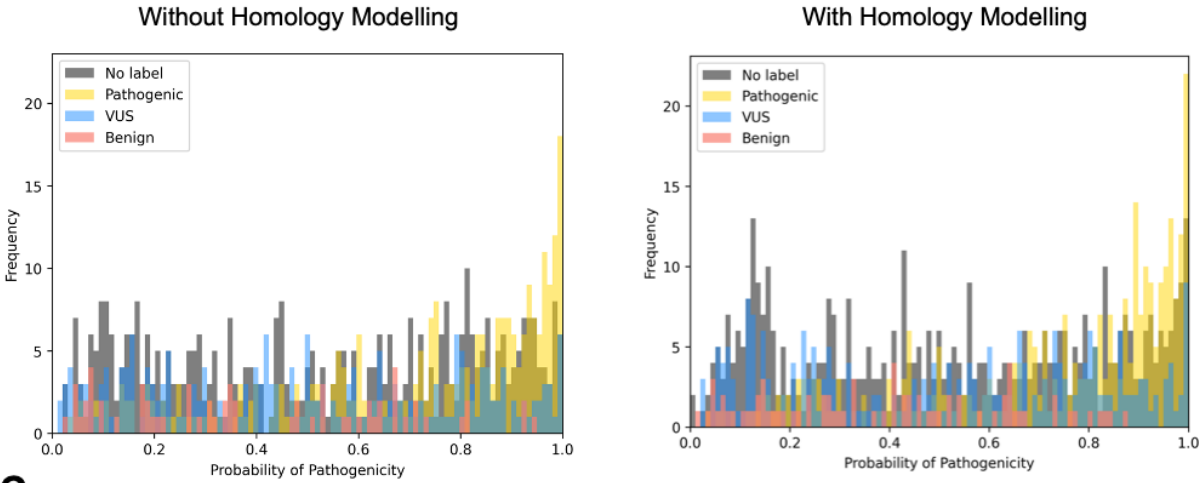

C.

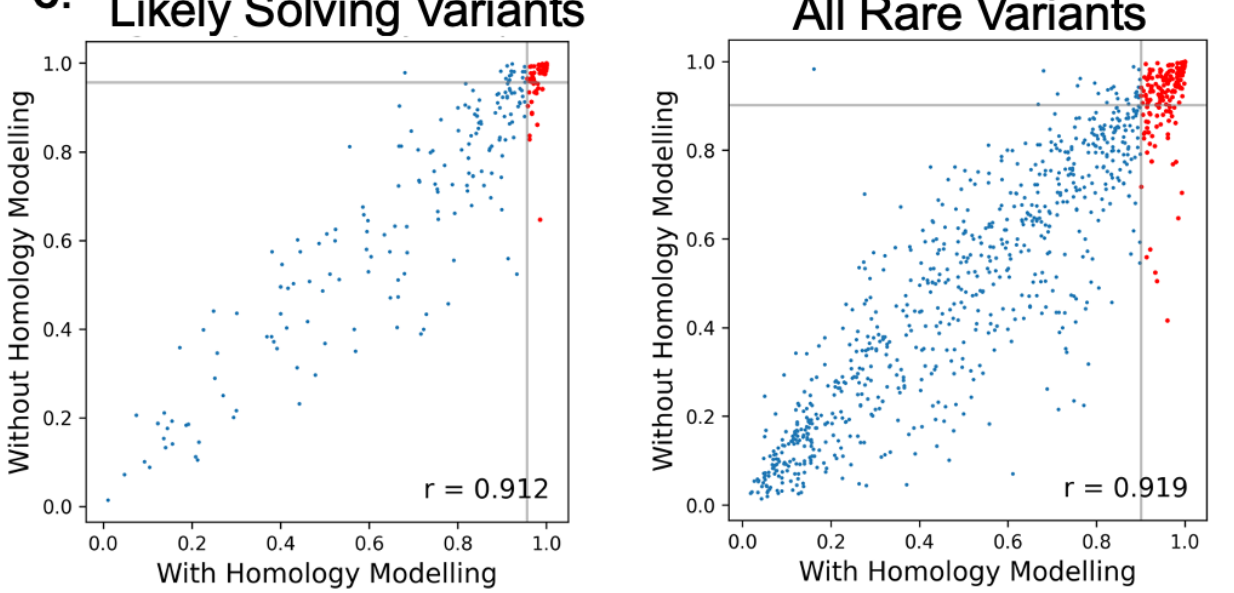

Figure S7. Unsolved patient variant pathogenicity probabilities are similar with and without homology modelling. Pathogenicity probability distributions by variant label for the **(A)** “likely solving variants” and **(B)** “all rare variants” datasets. **(C)** Pathogenicity probability comparisons with and without homology modelling. Red dots indicate variants that were included in the list of top hits for further analysis. Spearman correlation coefficients are show and are statistically significant with $p < 0.0001$.

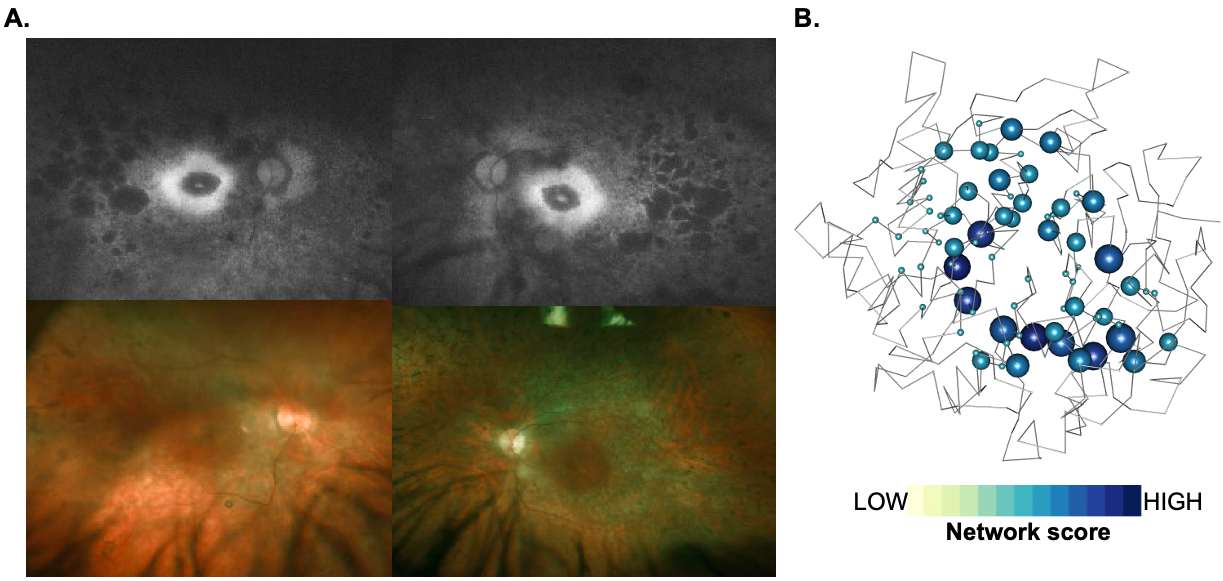

Figure S8. SBNA helps identify pathogenic variants in a patient with RPGR-related inherited retinal disease. Representation of network scores for a sample structure with putative solving genetic mutations. Sphere radius corresponds to network score magnitude at a particular position. A patient with clinical evidence of RPGR-related disease **(A)** but with no complete genetic explanation was fully solved using SBNA which highlighted a hemizygous mutation (Cys302Tyr) that score highly in the RPGR protein structure **(B)**.

Protein	PDB
AHI1	4ESR
ARL6	2H57
CNGA1	7LFT
CNNM4	6G52
CNNM4	6RS2
COL2A1	5NIR
GRK1	3C4Z
GUCA1A	2R2I
IMPDH1	7RER
INPP5E	2XSW
JAG1	4CC0
KIF11	1Q0B
KLHL7	3II7
MERTK	7AB0
NMNAT1	1KKU
OAT	1OAT
OFD1	6E0T
PRPF8	3ENB
RLBP1	3HY5
RP2	2BX6
RS1	3JD6
SNRNP200	4KIT
TUB	1S31
TULP1	3C5N
PTEN	1D5R
HRAS	4NIF
ABCA4	7LKZ
ABCC6	6BZS
ABCC6	6BZR
AIPL1	6PX0
CDH23	5TFM
CDH23	5WJ8
CDH23	5VVM
RPGR	4QAM
RPGRIP1	4QAM
CTNNA1	4IGG
CHM	1VG9
CHM	1VG0

CNGA3	7RHS
CNGB1	7RH9
CNGB3	7RHS
DFNB31	6KZ1
DFNB31	6FDD
DFNB31	6FDE
ERCC6	7OO3
GNAT1	1TND
GNAT1	1TAD
GNAT1	1TAG
IDH3B	6KDF
MYO7A	5MV9
MYO7A	3PVL
PCDH15	5ULY
PCDH15	6E8F
PCDH15	5T4M
PCDH15	4XHZ
PDE6A	6MZB
PDE6B	6MZB
PRPF3	6QW6
PRPF31	2OZB
RBP3	1J7X
RBP3	4LUR
TIMP3	3CKI
USH1C	3K1R
USH1G	3K1R
BRCA1	1JM7
BRCA1	1T29
ERK2	4FMQ
ERK2	4NIF
RPE65	3FSN
RPE65	3KVC
RPE65	4F2Z
RHO	1GZM
RHO	3CAP
PRPH2	7ZW1

Table S1. Protein Data Bank accession numbers for well-studied human proteins and IRD genes. Protein Data Bank[31] accession numbers listed here were used to access structural data for well-studied human proteins and IRD proteins.